Bulgarian Chemical Communications, Volume 47, Number 4 (pp. 1221 – 1228) 2015

Molecular simulation of protein transport controlled by pressure-driven flow in silica nanofluidic channels

K. Liu[1*], S. L. Chen[1], S. W. Xiao[2], X. L. Zhang[3], D. C. Ba[1*], D. Y. Wang[1], G. Y. Du[1], Y. S. Ba[1]

[1]*School of Mechanical Engineering and Automation, Northeastern University, Shenyang, 110089, China;*
[2]*Institute of High Energy Physics Chinese Academy of Sciences, 100049 Beijing, China;*
[3]*Capital Aerospace Machinery Company, Beijing, 100076, China*

Received April 4, 2015

A series of NEMD (non-equilibrium molecular dynamics) simulations were performed to study the biomolecular migration process driven by pressure in nanoscale channels. Several parameters, including channel height, driving pressure, system temperature and wall charge, were used to investigate the density and transport velocity of molecules and ions. The results show that the channel height has a significant influence on the distribution of density and velocity depended on the size of biomolecules. The wall charge density also greatly influences the velocity and ion concentration of proteins nearby the channel wall while the temperature only has a slight influence. The conclusions are useful to the design and manipulation of nanofluidic devices.

Key words: Molecular simulation, nanofluidic channel, protein molecules, transport process, NEMD, pressure-driven, nanoscale silica channels.

INTRODUCTION

Among the simulation techniques, EMD (equilibrium molecular dynamics) has been extensively applied to study the equilibrium fluid flow [11]. Meanwhile, for atomic systems far from equilibrium, NEMD (non-equilibrium molecular dynamics) offers an alternative method, especially in solving the nanofluidic problems [11-15]. In the nanofluidic field, electroosmosis and electrophoresis have been widely used to manipulate the fluid and biomolecules in simulations [16-24] and experiments [2, 25-28]. However, the flow can be driven by pressure in one direction unlike electricity-driven flow. There are some reports on modeling and numerical simulation of pressure-driven flow in the nanochannels [11-13, 15, 29-42]. While a single fluid is usually considered, biomolecule flows generated by pressure received less attention [43]. Some researchers have studied how the physical and geometric factors affected the biomolecular flux through the nanopores [43]. However, the interfacial interactions in the nanochannel have not been deeply explored. Besides, the factors affecting the transport of molecules and ions have not been completely understood yet.

The research purpose is to investigate the pressure-driven biomolecular flow in the nanochannel. This issue tries to analyze how the flow characteristics are influenced by the channel parameters. Before the simulations are started, β-cristobalite SiO_2 is selected as the channel wall while hen egg albumen lysozyme is selected as the biomolecule.

MODEL AND SIMULATION DETAILS

The simulation model is schematically presented in Fig.1, where the simulation region is regarded as a *3-D* box.

As shown in Fig.1, two silica walls are on the top and bottom, water molecules are hidden, three biomolecules are located in the central channel, blue and red spheres represent Na^+ and Cl^- ions respectively. The length L_x is 26.918 nm, the width L_z is 9.420 nm and the height L_y has five different values, namely, 8.438 nm, 9.438 nm, 10.438 nm, 11.438 nm and 12.438 nm for each system.

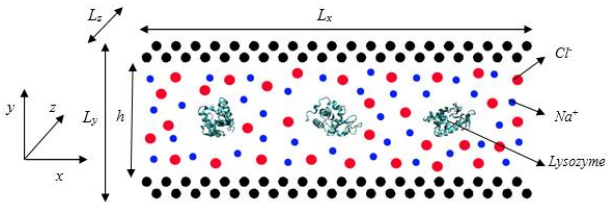

Fig.1. Cross-section of the simulation model for the pressure-driven flow

Table 1 lists the parameters including channel height *h*, driving acceleration α, temperature *T* and wall charge density ρ_{wall}. According to Table 1, a series of simulations have been performed. Periodic boundary conditions are imposed along *x* and *z* directions.

* To whom all correspondence should be sent:
E-mail: kliu@mail.neu.edu.cn (K. Liu),
dchba@mail.neu.edu.cn (D. C. Ba)

Table 1. Parameters of the simulation model.

No.	a (nm/ps^2)	ρ_{wall} (C/m^2)	h (nm)	T (K)
1	5.0	0.3	8.478	300
2	5.0	0.5	8.478	300
3	5.0	0.1	8.478	300
4	5.0	-0.1	8.478	300
5	5.0	-0.3	8.478	300
6	5.0	-0.5	8.478	300
7	5.0	0.3	6.478	300
8	5.0	0.3	7.478	300
9	5.0	0.3	9.478	300
10	5.0	0.3	10.478	300
11	2.0	0.3	8.478	300
12	8.0	0.3	8.478	300
13	5.0	0.3	8.478	320
14	5.0	0.3	8.478	340

Two silica substrates with identical surfaces are placed with the channel height along *y* direction. To simulate the real physical silica wall, the (111) crystallographic face of *β-cristobalite* SiO_2 is used as the silica wall [44]. To obtain a chemically realistic surface, all non-bridging oxygen atoms on the top of the *β-cristobalite* crystal are hydroxylated [45]. The *Si-O* bond is changed to the *Si-OH* bond in order that surface hydroxyl group density is 13.5 *OH*/nm^2.

The hydrogen atoms are positioned at 0.1 nm perpendicular to the surface. The wall atoms are kept around their original *fcc* lattice positions due to an elastic spring potential as following

$$u_{wall}\left(\left|r\left(t\right)-r_{eq}\right|\right)=\frac{1}{2}K\left(\left|r\left(t\right)-r_{eq}\right|\right)^2 \quad (1)$$

Where, *r(t)* is the position of an atom at time *t*, r_{eq} is its initial lattice position and *K* is the spring constant [11, 46]. This initial allows the wall molecules to vibrate, which could achieve the momentum transfer between fluid molecules and wall molecules. Here, *K* is set at 1000. The wall charge density ρ_{wall} is simulated with six cases: -0.5, -0.3, -0.1, 0.1, 0.3 and 0.5C/m^2.

Three hen egg albumen *lysozymes*, labeled as protein 1, protein 2 and protein 3, from left to right, are added in the center of the nanochannel with spacing of 9 nm and phase difference of 90 degrees. The *lysozyme* is positively charged with 8e. The water molecules are treated with *SPC/E* mode. The concentration of *NaCl* aqueous solution was as constant as 0.83 M throughout the whole simulation.

Because of the relatively large pressure drop in the nanochannels, an external large acceleration α (2, 5 and 8 nm/ps^2 for each case) is applied along the *x* direction to every fluid atom in order to simulate the real pressure-driven flow in the nanochannels. Flow energy caused by the pressure is converted into thermal energy absorbed by the wall atoms, resulting in an increase in system temperature [32]. Thus a velocity rescaling thermostat at the thermal walls is applied to keep the system temperature constant, described by:

$$\mathrm{d}K=(K_0\text{-}K)\frac{dt}{\Gamma T}+2\sqrt{\frac{KK_0}{N_{\mathrm{f}}}}\frac{dW}{\sqrt{\Gamma T}} \quad (2)$$

Where, *K* is the kinetic energy, N_f is the number of freedom degrees and *dW* is a *Wiener* process [47]. The system temperature *T* is kept constant at three values 300 K, 320 K and 340 K. The force field used here is the *charmm27* inside *Gromacs 4.5*. The *van der Waals* interactions are treated according to the 12-6 *Lennard-Jones* potential

$$V_{LJ}\left(r_{ij}\right)=\frac{C_{ij}^{(12)}}{r_{ij}^{12}}-\frac{C_{ij}^{(6)}}{r_{ij}^{6}} \quad (3)$$

The electrostatic forces are described by a coulombic potential with a cutoff set to 1.0 nm. Long-range interactions are calculated by the *PME* (particle mesh *Ewald*) method.

The simulation step time for the system is 2.0 fs. First of all, energy minimization is carried out. Then the system would reach equilibrium with a relaxation step at 1×10^5. Last, the *NEMD* simulation is performed with duration of 2×10^5 steps with an additional acceleration applied on each molecule.

RESULTS AND DISCUSSION

In order to solve the density and velocity distribution, the channel is divided into *n* bins along *z* direction. Then density and mean velocity are computed at each bin for all time steps and averaged upon 14 groups of parameters, as listed in Table 1.

Density and velocity distribution of water molecules

Fig.2 shows the water molecule density distribution along the height direction. Due to the strong solid–liquid interactions, the water molecules are distributed orderly near the solid interface. The distance between the first peaks and walls is about 0.3 nm, which is about the size of molecule diameter.

As shown in Fig.2(a), two peaks of water density are observed near the solid interface at the channel height of 9.478 nm and 10.478 nm. With decreasing channel height, the number of peak increases to three and the newly appeared peak becomes more obvious and closer to the wall. The oscillatory characteristics of water molecular density near the walls change drastically with the decreasing of channel height *h* under 8.478 nm. On the contrary, the layered water molecular density near the walls becomes stable above 8.478 nm.

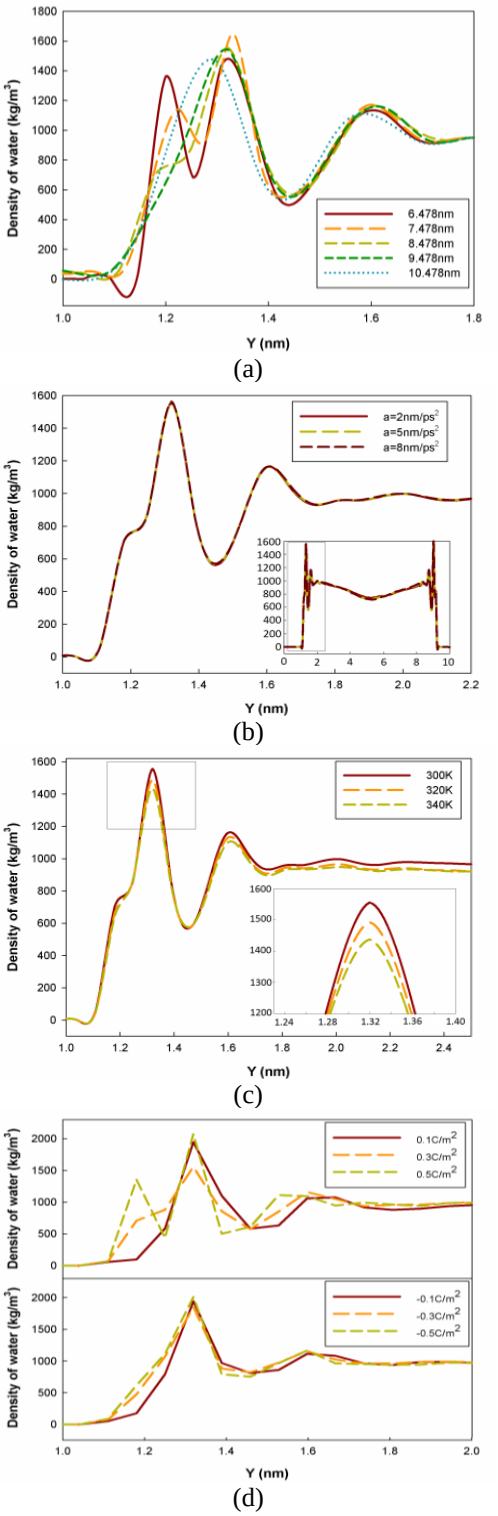

Fig. 2. Density distribution of water molecules at h=8.478 nm, $\vec{a}$ =5 nm/ps^2, T=300K and ρ_{wall}=0.3C/m^2 (unless otherwise stated), (a) at h=6.478, 7.478, 8.478, 9.478 nm and 10.478 nm, (b) at $\vec{a}$ =2, 5 and 8 nm/ps^2, (c) at T=300, 320 and 340K, (d) at ρ_{wall}=-0.5, -0.3, -0.1, 0.1, 0.3 and 0.5 C/m^2.

In Fig.2(b) we examine the pressure influence on water molecular density by exerting acceleration on all molecules. The central water molecular density only decreases marginally with the acceleration while the density near the wall seldom changes. The similar situation is observed in Fig.2(c), which is used to examine the influence of temperature (from 300 to 340K) on water molecular density profile. The central water molecular density is marginally increasing with the temperature. Besides, the two distinct peaks are very close to the wall interface, which decrease with the temperature.

Fig.2(d) summaries the influences of wall surface charge on density. When the wall is positively charged, the water density near the wall reaches the peaks twice when ρ_{wall} equals 0.1C/m^2, while it reaches three times when ρ_{wall} equals 0.5C/m^2. In fact, the additional peak is closer to the wall. However, the situation is quite different when the wall is negatively charged. Both the peak number and the value change little with the charges. The different mass of the hydrogen and oxygen atoms could be considered as the cause. The oxygen ions are adsorbed to the wall when the wall is positively charged while the hydrogen ions are adsorbed when the wall is negatively charged. However, the mass of the oxygen atoms is 16 times that of the hydrogen, so a new peak will appear near the positively charged wall.

The water velocity distribution along the height direction was calculated and shown in Fig.3, which is similar to *Poiseuille* distribution. The center is high due to the small resistance here. Furthermore, the closer the water molecules are to the wall, the stronger are the solid-fluid interactions while the smaller is the water velocity.

The influence of channel height on water molecular velocity is shown in Fig.3(a): when *h* equals 6.478 nm, the velocity in the channel center is the highest, and the velocity difference between layers close to walls is also the largest. Although the velocity and the differences decrease with *h*, they become negligible when *h* increases to 9.478. This states that the channel height has a great influence on the velocity of water molecules under 8.478 nm. Increased velocity was also observed when the pressure increases, as shown in Fig.3(b). The kinetic energy of water molecules increases with the exerted acceleration, so does the velocity.

The influences of temperature on water molecular velocity are also examined, as shown in Fig.3(c). It shows that the influences are so complicated that no rules can explain the changes. However, these results could be understood when considering the thermal motion of water molecules under different temperatures. Due to the disorder of thermal motion, the profile of the temperature influencing the water velocity is irregular. The similar situation happens as shown in Fig.3(d) which examines the influence of wall charge density on

water molecular density.

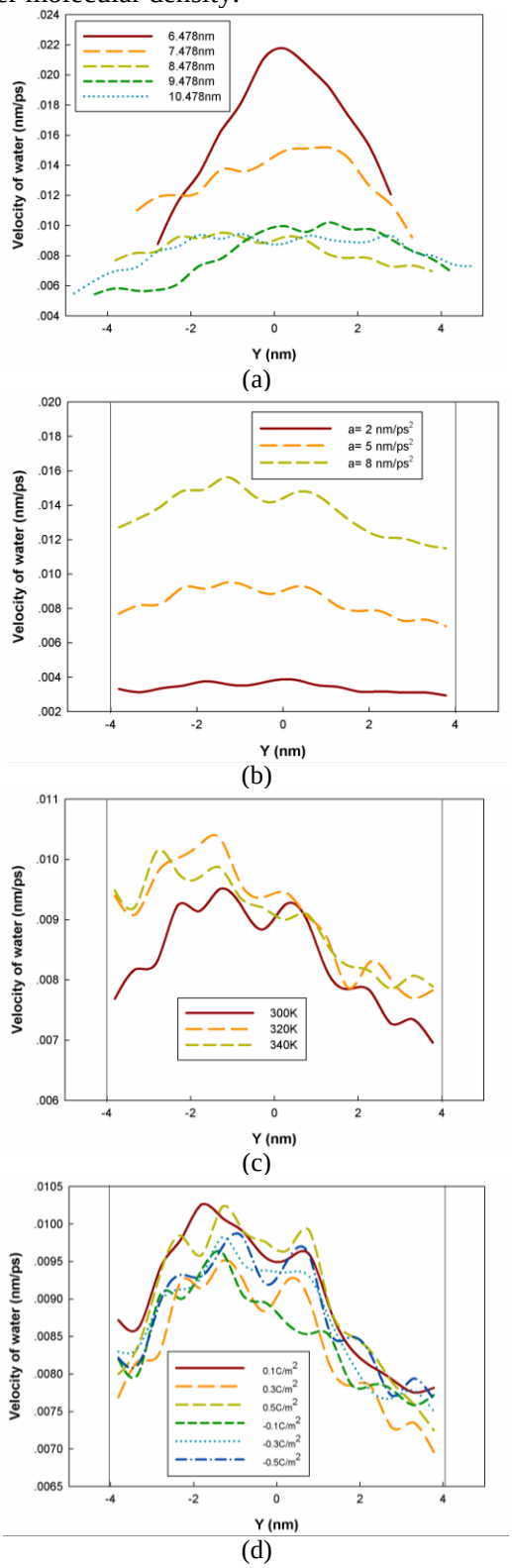

Fig. 3. Velocity distributions of water at h=8.478 nm, $\vec{a}$ =5 nm/ps^2, T=300K and ρ_{wall}=0.3C/m^2 (unless otherwise stated), (a) at h=6.478, 7.478, 8.478, 9.478 nm and 10.478 nm, (b) at $\vec{a}$ =2, 5 and 8 nm/ps^2, (c) at T=300, 320 and 340K, (d) at ρ_{wall}=-0.5, -0.3, -0.1, 0.1, 0.3and 0.5C/m^2.

Ion concentration distribution

Fig.4 shows the ion concentration distribution along the channel height direction. Due to the strong electrostatic interactions, the co-ions are mainly located in the central channel while the counter-ions are mainly adsorbed to the channel wall.

In Fig.4(a)~(b), we examine the influence of channel height on ion concentration. The ions distribution is uneven with a distinct peak when *h* equals 6.478 nm. On the contrary, the distribution becomes uniform when *h* increases to 7.478 nm. However, two unobvious peaks appear in both sides of the center with the increasing of *h*. This is mainly because three positively charged *lysozyme* molecules in the center will stay away from the Na^+ ions. As shown in Fig.4(b), two distinct peaks appear near the wall when *h* equals 6.478 nm. However, the peak number decreases to one with *h*. The peaks of Cl^- ion concentration decrease with *h*, but they hardly change above 8.478 nm.

As shown in Fig.4(c)~(d), the influence of pressure on ion concentration is negligible. The similar situation happens in Fig.4(e)~(f) showing the temperature's influence on ion concentration. Moreover, increasing of Cl^- ion concentration with temperature is shown in Fig.4(f).

The wall charge density's influence on ion concentration is shown in Fig.4 (g)~(j). With the increase in absolute wall charge density, more co-ions are repelled to the center. When the ion concentration in the center increases, ion concentration distribution becomes more uneven. As shown in Fig.4(h), there is only one peak of Cl^- ion concentration close to the wall due to the wall electrostatic interactions. Meanwhile, the distance between the peak and wall decreases with the positive wall charge density. However, the peak increases. On the other hand, when the wall is negatively charged, the situation becomes complicated. The Na^+ ion concentration reaches the peak when ρ_{wall} equals -0.1C/m^2. It has three peaks at -0.3C/m^2 and two peaks at -0.5C/m^2. Moreover, the similar phenomena happen in Fig.4(j), the distance between the peak of Na^+ ion concentration and the wall decreases with the negative wall charge density. However, the peak increases.

Biomolecular density and velocity distribution

Due to the complexity and high surface activity of the biomolecules, the effect of the parameters (*h*, $\vec{a}$,*T*, ρ_{wall}) on the biomolecular movements becomes very complicated. Fig.5 shows the biomolecular density distribution along the height direction. As shown in Fig.5, the lysozyme biomolecules are mainly located in the center.

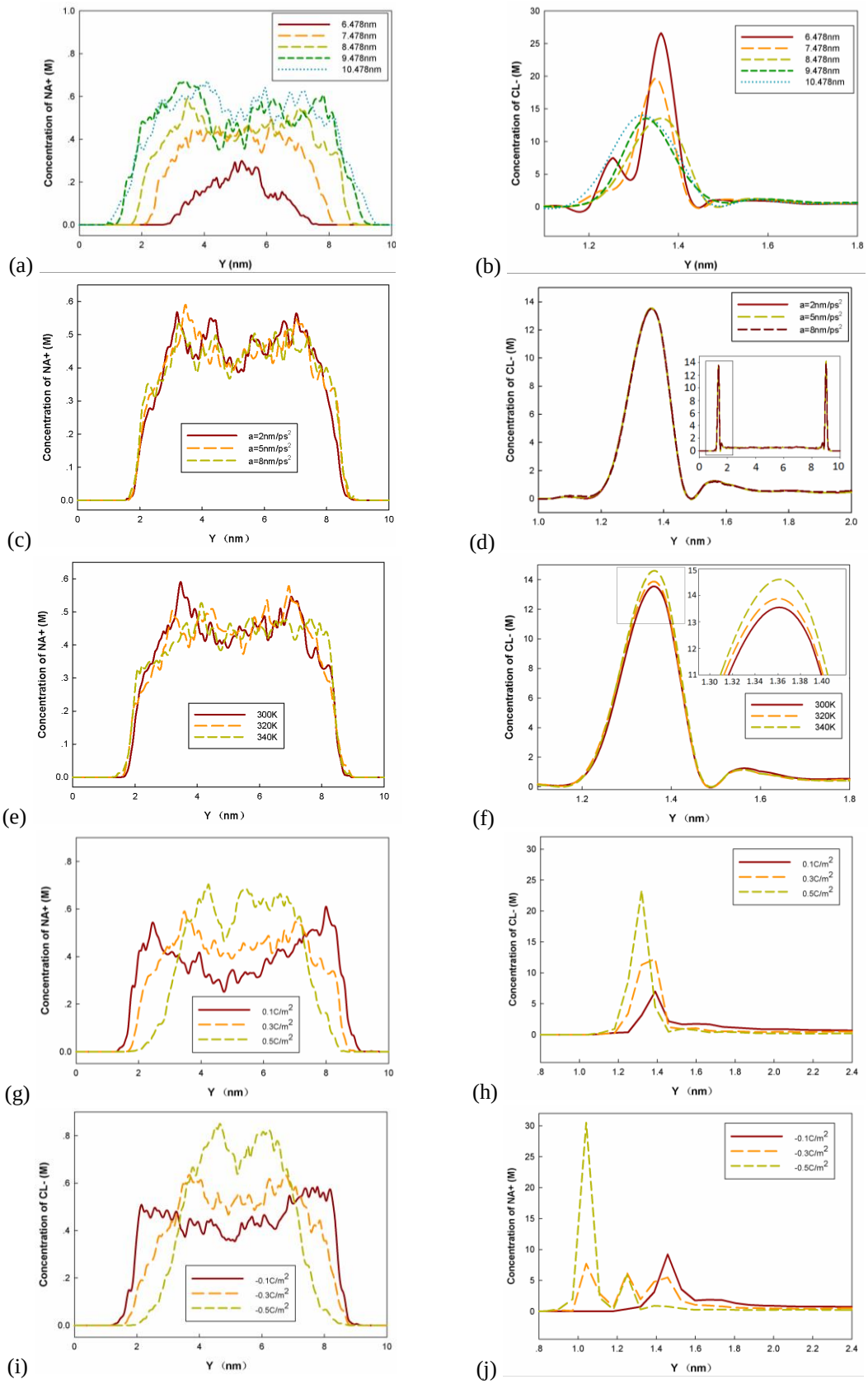

Fig. 4. Concentration distributions of ions at h=8.478 nm, $\vec{a}$ =5 nm/ps^2, T=300K and ρ_{wall}=0.3 C/m^2 (unless otherwise stated), (a) (b) at h=6.478, 7.478, 8.478, 9.478 nm and 10.478 nm, (c) (d) at $\vec{a}$ =2, 5 and 8 nm/ps^2, (e) (f) at T=300, 320 and 340K, (g) (h) at ρ_{wall}= 0.1, 0.3 and 0.5C/m^2, (i) (j) at ρ_{wall}= -0.1, -0.3, and -0.5 C/m^2.

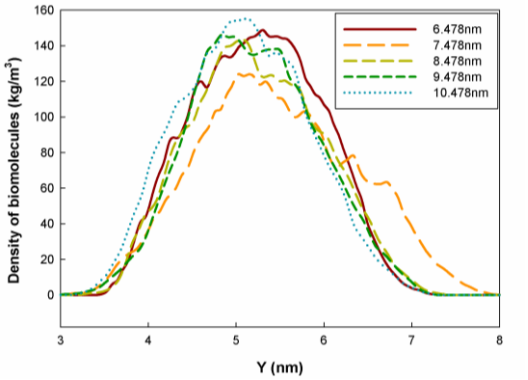

(a)

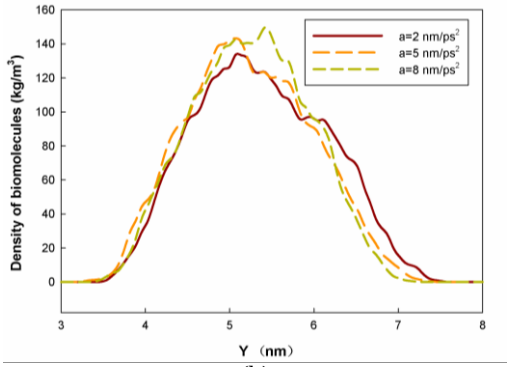

(b)

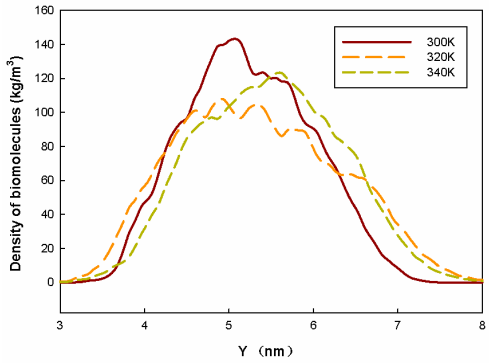

(c)

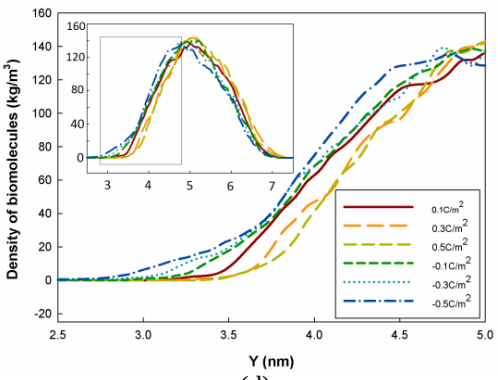

(d)

Fig. 5. Biomolecular density distribution at h=8.478 nm, $\vec{a}$ =5 nm/ps^2, T=300K and ρ_{wall}=0.3 C/m^2 (unless otherwise stated), (a) at h=6.478, 7.478, 8.478, 9.478 nm and 10.478 nm, (b) at $\vec{a}$ =2, 5 and 8 nm/ps^2, (c) at T=300, 320 and 340K, (d) at ρ_{wall}=-0.5, -0.3, -0.1, 0.1, 0.3 and 0.5 C/m^2.

As shown in Fig.5(a), the channel height's influence on biomolecular density is unpredictable. The similar situation happens in Fig.5(c), which shows the temperature's influence on biomolecular density. The pressure effect on biomolecular density is summarized in Fig.5(b), which shows that it increases with the acceleration peaking at 8 nm/ps^2. Because greater pressure exerted on the biomolecules brings greater speeds and resistance, the biomolecules have to shrink their shape, which leads to high biomolecular density in the middle.

Fig. 5(d) shows the influence of wall charge density on biomolecular density. The distance between the wall and biomolecules increases with the wall charge density from -0.5 to 0.5 C/m^2. As a result, the positively charged biomolecules are attracted by the negatively charged wall or excluded by the positively charged wall. However, either the attractive force or repulsive force increases with the wall charge density.

Fig. 6 shows the average velocity of three lysozyme biomolecules in the channel numbered with *p1*, *p2* and *p3*. Among them, *p1* has the lowest velocity and *p2* has the highest velocity.

Fig. 6(a) shows the channel height's influence on biomolecular velocity. It shows that the biomolecular velocity decreases with *h* and reaches the peak point at 6.478 nm. As the water molecular velocity decreases with channel height, the biomolecular velocity also decreases with channel height. Moreover, the velocity increments of biomolecules become smaller with the increase in channel height above 8.478 nm, so the height's influence on biomolecular velocity becomes less important with the increase. Fig. 6(b) shows the pressure's influence on biomolecular velocity. As the water molecular velocity increases with acceleration, the biomolecular velocity increases linearly.

Fig. 6(c) shows the temperature's influence on biomolecular velocity. As the disorder of thermal motion increases with temperature, biomolecular velocity slightly decreases except for *p2* at 340K.

Fig. 6(d) shows the influence of wall charge density on biomolecular velocity. It shows that the biomolecular velocity increases marginally with the absolute wall charge density. As a fact, the central water molecules face the smallest resistance, so this velocity is greater than that nearby the wall. Due to the attractive or compulsive force induced by the charged wall, more biomolecules are limited in the central channel with the increase in the wall charge

density. Thus the greater the absolute wall charge density, the higher is the biomolecular velocity. However, this influence is much smaller than the pressure's, which results in a slight increase of the biomolecular velocity.

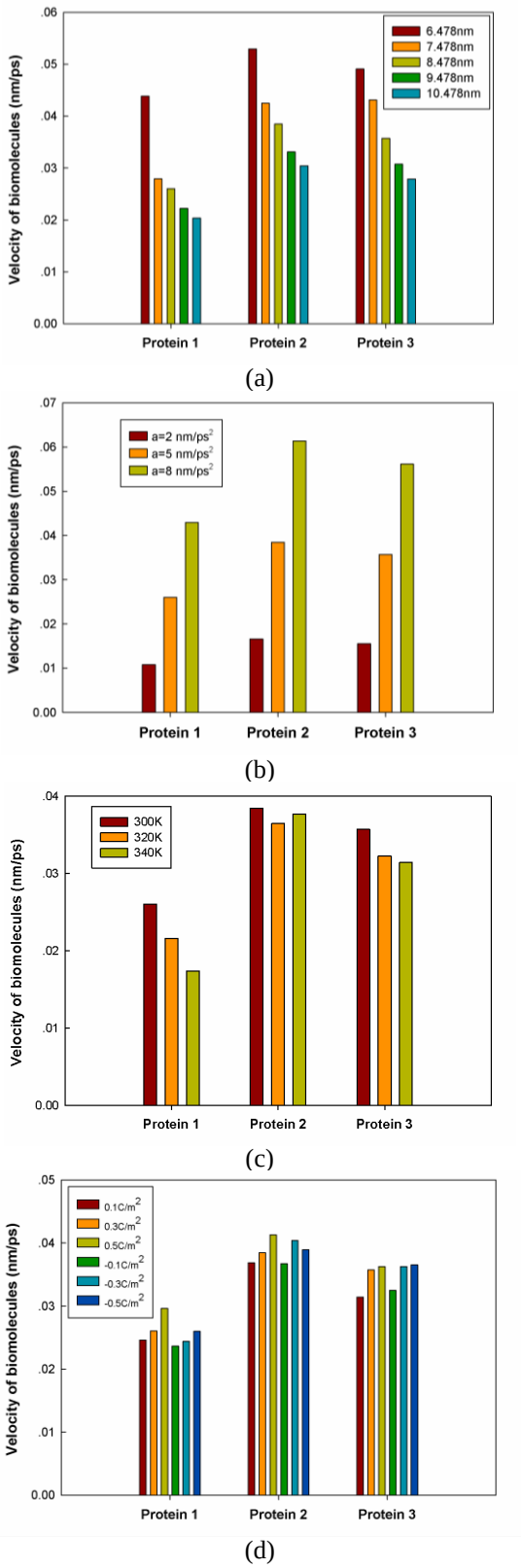

Fig. 6. Velocity distribution of biomolecules at h=8.478 nm, $\vec{a}$ =5 nm/ps^2, T=300K and ρ_{wall}=0.3 C/m^2 (unless otherwise stated), (a) at h=6.478, 7.478, 8.478, 9.478 nm and 10.478 nm, (b) at $\vec{a}$ =2, 5 and 8 nm/ps^2, (c) at T=300, 320 and 340K, (d) at ρ_{wall}=-0.5, -0.3, -0.1, 0.1, 0.3 and 0.5 C/m^2.

CONCLUSIONS

The *NEMD* simulation of biomolecular flows in a SiO_2 nanochannel driven by pressure is presented. The results show that the interfacial interactions play an important role in determining the transport characteristics of ions, water molecules and biomolecules in the nanochannel. The following conclusions can be drawn from the present simulation. First, the change in water molecular density and ion concentration close to the wall becomes sharper with the decrease in channel height under 8.478 nm while the molecular velocity decreases with the channel height. Second, the velocity of water molecules and biomolecules linearly increases with the exerted acceleration. Third, the characteristics near the walls are slightly influenced by the temperature. Last, the wall charge density greatly affects the ion concentration distribution, but not the water molecular velocity.

As the channel height and wall charge density are decisive to the density distribution, they should be carefully chosen in designing nanofluidic devices. Besides, the system temperature should also be considered.

Acknowledgements: *This work has been jointly supported by the National Natural Science Foundation of China (51376039), the Doctoral Fund of Ministry of Education of China (20120042110031) and the Fundamental Research Funds for the Central Universities of China (N120403006).*

REFERENCES

1. R. Karnik, K. Castelino, R. Fan, P. D. Yang, A. Majumdar, *NanoLett.*, **5**, 1638 (2005).
2. R. Karnik, R. Fan, M. Yue, D. Y. Li, P. D. Yang, A. Majumdar, NanoLett. **5**, 943 (2005).
3. R. Karnik, K. Castelino, *Appl. Phys. Lett.*, **88**, 123114 (2006).
4. E. Tamaki, A. Hibara, H. B. Kim, M. Tokeshi, T. Kitamori, *J. Chromatogr. A*, **1137**, 256 (2006).
5. J. Fu, R. B. Schoch, A. L. Stevens, S. R. Tannenbaum, J. Han, *Nature Nanotech.*, **2**, 121 (2007).
6. N. Douville, D. Huh, S. Takayama, Anal Bioanal Chem., **391**, 2395 (2008).
7. T. Tsukahara, K. Mawatari, A. Hibara, T. Kitamori, *Anal Bioanal Chem.*, **391**, 2745 (2008).
8. M. A. G. Zevenbergen, B. L. Wolfrum, E. D. Goluch, P. S. Singh, S. G. Lemay, *J. AM. CHEM. SOC.*, **131**, 11471 (2009).
9. M. Ben Ishai, F. Patolsky, *J. AM. CHEM. SOC.*, **131**, 3679 (2009).

10. D. Frenkel, B. Smit, Understanding Molecular Simulation: from Algorithms to Applications, Academic Press, San Diego, 1996.
11. F. Sofos, T. Karakasidis, A. Liakopoulos, *Int. J. Heat Mass Transfer*, **52**, 735 (2009).
12. F. Sofos, T. E. Karakasidis, A. Liakopoulos, *Contemporary Engineering Sciences*, **2**, 283 (2009).
13. G. González, J. C. Tejas, J. P. A. Vallejo, J. F. J. Alvarado, O. Manero, *Rheol. Acta*, **48**, 1017 (2009).
14. F. Sofos, T. E. Karakasidis, A. Liakopoulos, *Int. J. Heat Mass Transfer*, **53**, 3839 (2010).
15. D. T. Semiromi, A. R. Azimian, *Heat Mass Transfer*, **46**, 791 (2010).
16. J. W. Kanga, K. R. Byuna, J. Y. Lee, S. C. Kong, Y. W. Choi, H. J. Hwang, *Physica E*, **24**, 349 (2004).
17. R. Qiao, N. R. Aluru, *Colloids and Surfaces A: Physicochem. Eng. Aspects*, **267**, 103 (2005).
18. R. Qiao, *Langmuir*, **22**, 7096 (2006).
19. R. Qiao, *MicrofluidNanofluid*, **3**, 33 (2007).
20. S. M. Cory, Y. Liu, M. I. Glavinović, *Biochim. Biophys. Acta*, **1768**, 2319 (2007).
21. D. Duong-Hong, J. S. Wang, G. R. Liu, Y. Z. Chen, J. Han, N. G. Hadjiconstantinou, *MicrofluidNanofluid*, **4**, 219 (2008).
22. C. D. Lorenz, P. S. Crozier, J. A. Anderson, A. Travesset, *J. Phys. Chem. C*, **112**, 10222 (2008).
23. Y. S. Choi, S. J. Kim, *J. Colloid Interface Sci*., **333**, 672 (2009).
24. E. C. Yusko, R. An, M. Mayer, *ACS Nano*, **4**, 477 (2010).
25. A. Plecis, R. B. Schoch, P. Renaud, *Nano Lett*., **5**, 1147 (2005).
26. Y. Liu, K. Oh, J. G. Bai, C. Chang, W. Yeo, J. Chung, K. Lee, W. K. Liu, *Comput. Methods Appl. Mech. Engrg*.,**197**, 2156 (2008).
27. Y. J. Oh, A. L. Garcia, D. N. Petsev, G. P. Lopez, S. R. J. Brueck, C. F. Ivoryc, S. M. Han, *Lab Chip.*, **9**, 1601 (2009).
28. U. Vermesh, J. W. Choi, O. Vermesh, R. Fan, J. Nagarah, J. R. Heath, *Nano Lett.*, **4**, 1315 (2009).
29. D. T. W. Lin, C. K. Chen, *Acta Mech*., *173*, 181 (2004).
30. S. Das, T. Das , S. Chakraborty, *Sens. Actuators B*, **114**, 957 (2006).
31. D. T. W. Lin, *Int. J. Biol. Macromol*., 41, 260 (2007).
32. A. Ghosh, R. Paredes, S. Luding, Poiseuille flow in a nanochannel–use of different thermostats, (PARTEC 2007–International Congress on Particle Technology).
33. F. H. J. van der Heyden, D. J. Bonthuis, D. Stein, C. Meyer, C. Dekker, *Nano Lett*., 7, 1022 (2007).
34. X. J. Gong, J. Y. Li, H. Zhang, R. Z. Wan, H. J. Lu, S. Wang, H. P. Fang, *Phys. Rev. Lett*., **101**, 257801 (2008).
35. M. Cieplak, *Eur. Phys. J. Spec. Top*., **161**, 35 (2008).
36. Y. H. Wu, B. Wiwatanapataphee, M. B. Hu, *Physica A*, **387**, 5979 (2008).
37. S. Joseph, N. R. Aluru, *NanoLett.*, **8**, 452 (2008).
38. J. Goldsmith, C. C. Martens, *J. Phys. Chem. Lett.*, **1**, 528 (2010).
39. A. Szymczyk, H. Zhu, B. Balannec, *Langmuir*, **26**, 1214 (2010).
40. J. A. Thomas, A. J. H. McGaughey, O. Kuter-Arnebeck, Int. J. Therm. Sci., 49, 281 (2010).
41. H. Hoang, S. Kang, Y. K. Suh, *J. Mech. SCI. Technol*., **24**, 1401 (2010).
42. Y. X. Li, J. L. Xu, D. Q. Li, *MicrofluidNanofluid*, **9**, 1011 (2010).
43. G. De Luca, M. I. Glavinović, *Glutamate*, *Biochim. Biophys. Acta*, **1768**, 264 (2007).
44. W. W. Schmahl, I. P. Swainson, M. T. Dove, A. G-Barber, *Z. Kristallogr.*, **201**, 125 (1992).
45. D. Argyris, D. R. Cole, A. Striolo, *ACS Nano*, **4**, 2035 (2010).
46. R. Kamali, A. Kharazmi, *Int. J. Therm. Sci.*, **50**, 226 (2011).
47. G. Bussi, D. Donadio, M. Parrinello, *J. Chem. Phys*., **126**, 014101 (2007).

МОЛЕКУЛНО СИМУЛИРАНЕ НА ТРАНСПОРТА НА ПРОТЕИНИ, КОНТРОЛИРАН ЧРЕЗ ПОТОК, ЗАДВИЖВАН ЧРЕЗ НАЛЯГАНЕ В НАНО-КАНАЛИ ОТ СИЛИЦИЕВ ДИОКСИД

К. Лю[1,*], Ш. Л. Чен[1], Ш. У. Ксиао[2], С. Л. Жанг[3], Д. Ч. Ба[1,*], Д. Я. Ванг[1], Г. Ю. Ду[1], Я. Ш. Ба[1],

[1]*Училище по машинно инженерство и автоматика, Североизточен университет, Шенгянг, Китай*
[2]*Институт по физика на високите енергии, Китайска академия на науките, Бейджин, Китай*
[3]*Столична компания за космическо машиностроене, Бейджин, Китай*

Постъпила на 4 април, 2015 г.

(Резюме)

В серия от симулации с неравновесна молекулна динамика (NEMD) са изследвани процесите на би-молекулна миграция, предизвикана от налягане в канали с нано-размери. Използвани са различни параметри, включително височина на каналите, налягане, температура и заряд на стените за изследването на плътността и скоростта на транспорт на молекули и йони. Резултатите показват, че височината на каналите има значително въздействие върху плътността и скоростта в зависимост от размера на био-молекулите. Плътността на заряда също влияе силно на скоростта и йонната концентрация в близост до стените на канала, докато температурата има слабо влияние. Направените зводи са полезни при конструирането на уреди с нано-флуиди.